Estimation of the Sea Surface Radar Cross Section at HF from Second-Order Doppler Spectrum Characteristics

D. B. TRIZNA

Radar Techniques Branch
Radar Division

May 25, 1982

NAVAL RESEARCH LABORATORY
Washington, D.C.

82 06 07 033

REPORT DOCUMENTATION PAGE		READ INSTRUCTIONS BEFORE COMPLETING FORM
1. REPORT NUMBER NRL Report 8579	2. GOVT ACCESSION NO. AD-A115 230	3. RECIPIENT'S CATALOG NUMBER
4. TITLE (and Subtitle) ESTIMATION OF THE SEA SURFACE RADAR CROSS SECTION AT HF FROM SECOND-ORDER DOPPLER SPECTRUM CHARACTERISTICS		5. TYPE OF REPORT & PERIOD COVERED Interim report on a continuing NRL Problem.
		6. PERFORMING ORG. REPORT NUMBER
7. AUTHOR(s) D. B. Trizna		8. CONTRACT OR GRANT NUMBER(s)
9. PERFORMING ORGANIZATION NAME AND ADDRESS Naval Research Laboratory Washington, DC 20375		10. PROGRAM ELEMENT, PROJECT, TASK AREA & WORK UNIT NUMBERS 61153 RR021-05-43 53-1515-0-2
11. CONTROLLING OFFICE NAME AND ADDRESS Department of Navy Office of Naval Research Arlington, VA 22217		12. REPORT DATE May 25, 1982
		13. NUMBER OF PAGES 24
14. MONITORING AGENCY NAME & ADDRESS(if different from Controlling Office)		15. SECURITY CLASS. (of this report) UNCLASSIFIED
		15a. DECLASSIFICATION/DOWNGRADING SCHEDULE
16. DISTRIBUTION STATEMENT (of this Report) Approved for public release; distribution unlimited.		
17. DISTRIBUTION STATEMENT (of the abstract entered in Block 20, if different from Report)		
18. SUPPLEMENTARY NOTES		
19. KEY WORDS (Continue on reverse side if necessary and identify by block number) HF radar Sea clutter Radar Doppler spectra Radar cross section		

20. ABSTRACT (Continue on reverse side if necessary and identify by block number)

A technique is developed for estimating the radar cross section of the sea surface at HF (2-30 MHz) from two simple measurements made of the radar Doppler spectrum. These are: the ratio of approach/recede Bragg line energy, and the ratio of strongest Bragg line amplitude to average value amplitude of second-order backscatter at zero Doppler frequency. A nomograph is given, based on a theoretical model of second-order scatter developed by the author, which then allows one to determine the number of decibels the Bragg ocean spectral component is down from the

(Continued)

DD $_{1 \text{ JAN } 73}^{\text{FORM}}$ 1473   EDITION OF 1 NOV 65 IS OBSOLETE
S/N 0102-014-6601

i

20. ABSTRACT (Continued)

classical Phillips asymptotic value, used here only for a reference. Comparison is made with some surface wave data for three different cases in which buoy data are available for comparison with multi-frequency radar data collected simultaneously at two different look angles. An example is also shown where such a calculation can be used to estimate the cross section of a target return existing within the same Doppler spectrum. Limitations of the technique are also discussed.

CONTENTS

DTIC
COPY
INSPECTED
2

Accession For

NTIS GRA&I	X
DTIC TAB	□
Unannounced	□
Justification	

By___
Distribution/

Availability Codes

| Dist | Avail and/or Special |
| A | |

ESTIMATION OF THE SEA SURFACE RADAR CROSS SECTION AT HF FROM SECOND-ORDER DOPPLER SPECTRUM CHARACTERISTICS

INTRODUCTION

The radar scattering coefficient of the sea surface at HF, σ^0, is generally difficult to obtain by a straightforward well-calibrated radar measurement because several of the variables used in the radar equation are not well known. For either surface wave or skywave illumination of the sea surface, the gain to be used in the radar equation is difficult to estimate because it can be a complex function of local ground, soil moisture, ground screen quality, coupling to the sea surface, tidal effects, and so on. For the case of a skywave measurement the problem is further compounded by the variation of the gain with elevation angle, as well as the ionospheric propagation losses the signal suffers within the ionosphere in its two refractive passes.

Knowledge of σ^0 of the sea by a means independent of the radar equation would allow one to determine the unknowns discussed above, as well as prove useful for comparison with targets which might be detected in the Doppler spectrum one is measuring. This would allow one, for example, to attempt to apply target identification techniques to the target of interest. These have been developed over the past several years by Ksiensky and others at the Ohio State University Electroscience Laboratory and are particularly applicable to the HF band of radar frequencies [1]. These techniques depend upon a multi-parameter measurement of a target and a comparison of that measurement with a catalog of values of cross section as a function of the parameters available. The parameters in question typically include radar frequency, polarization and phase. For ionospheric propagation, radar frequency can be varied over a reasonable bandwidth for coverage of a given illuminated area, of the order of 6 MHz. For the elliptically polarized wave which exits the ionosphere, a measurement of the difference between the minima and maxima in signal amplitude can be used to draw some conclusions about the ratio of horizontal to vertical radar cross section of a target. Phase information in an absolute or even relative sense between two radar frequencies is not known for ionospheric propagation. Hence, with some information about two of the three parameters available, target identification with skywave HF radar might be possible with a satisfactory calibration cross section for comparison, such as that of the sea surface.

Another application of such cross section information is that of remote sensing of the sea surface. It is well known that, to first order, the cross section of the sea surface is proportional to the components of the ocean wave directional energy spectrum which are travelling toward and away from the radar bearing. Hence, assuming one knows or can estimate the directional spreading of the wave spectrum, one can then determine how highly the sea surface is developed. Coupled with knowledge of the longest wavelengths excited, and an estimate of wave spreading with angle, one can get a good estimate of RMS waveheight.

In the following sections we test a simple scheme for estimating the radar cross section of the sea using a measurement of relative amplitudes of the approach and recede Bragg lines, in addition to the relative amplitude of second-order energy around zero Doppler frequency. By using a nomograph based on a theoretical model for the radar Doppler spectrum and these measurements, a value of σ^0 is obtained. Some comparisons are made with surface wave Doppler spectra for which surface truth ocean

wave spectra are available. The assumptions made in the theory are discussed in light of the comparison. The technique is particularly useful in the sense that it can deal with cases in which the actual prevailing ocean wave spectrum may have severe departures from idealized spectra (such as the Pierson-Moskowitz or JONSWOP models), which is in fact the case for several of the data comparisons. The key to this technique is that both radar measurements used are a function of wave components in nearly the same region of frequencies of the wave spectrum, and are not dependent upon the long wavelength regions which contribute heavily to the total energy of the ocean wave spectrum, and in which much of the amplitude variability may occur. It is noted that the empirical technique developed in Ahearn et al. [2] is similar to the one developed here, except for directional effects and an absolute calibration.

FIRST-ORDER BRAGG SCATTER

The integrated or total radar cross section measured by a Doppler radar is defined by the equation:

$$\sigma^0 = 1/2 \int_{-\infty}^{\infty} \sigma^0(\omega) \, d\omega = \int_0^{\infty} \sigma^0(\omega) \, d\omega, \tag{1}$$

where ω is the radio frequency in radians. In operating a pulse-Doppler radar with a given receiver band pass filter, the integrand of Eq. (1) is multiplied by the filter function describing the filter, which effectively changes the limits of integration to the upper and lower frequencies of the pass band. Since the radar is operated at some pulse repetition frequency, or PRF, the sampling theorem effectively folds the energy contained in the pass band filter into a narrower bane of frequency equal to that of the radar PRF, generally tens of hertz for an HF radar. The PRF is typically chosen so as to contain all of the scattered radar energy of interest in an unambiguous manner in Doppler. The result is that the limits of integration of Eq. (1) can be further reduced to that of plus and minus one half of the PRF. The variable of integration is now Doppler frequency, ω_D. (Unless further filtering is done, the noise power rises within the PRF bandwidth by a factor equal to the ratio of receiver filter pass bandwidth divided by the PRF, assuming it is white noise across the pass band. We are not concerned with noise here so we shall ignore this effect hereafter.)

The term within the kernel of Eq. (1) is referred to as the scattering cross section per unit frequency, or scattering cross section, as opposed to the total or integrated cross section on the left-hand side. For sea scatter at HF, it can be expanded into first, second, and higher order contributions in the following manner:

$$\sigma^0(\omega_D) = \sigma^0_{(1)}(\omega_D) + \sigma^0_{(2)}(\omega_D) + \ldots . \tag{2}$$

where the two terms on the right side are the first- and second-order contributions to the radar cross section.

The relationship of the first-order approach-recede Bragg line contributions to the radar Doppler spectrum with the wind driven ocean wave spectrum is:

$$\sigma^0_{(1)}(\theta, \omega_D) = 8 \pi K_B^4 [S(K_B, \theta) \delta(\omega_D + \omega_B) + S(K_B, \theta + \pi) \delta(\omega_D - \omega_B)], \tag{3}$$

where $S(K_B, \theta)$ is the directional ocean wave spectrum; θ is the angle between the transmitted radar vector and the wind direction; K_B is the Bragg resonant ocean wave number, related to the radar wave number, k, by $K_B = 2k \sin \phi$; ϕ is the angle between the normal and incident (and scattered) radio wave; and $\omega_B = \Omega_B = \sqrt{g K_B}$ is the Bragg Doppler frequency, equal to the ocean wave Bragg frequency. Barrick [3] derived Eq. (3) for HF applications, and a surface wave experiment by Teague et al. [4], verified the theory to within 3 dB accuracy. That experiment made use of measurement of energy backscattered from the sea made simultaneously with energy received from the transmit site, a LORAN C station. Hence, antenna gains of both the transmitter and receiver cancel one another when taking a ratio of radar equations for both paths (received power for the direct path divided by received power for sea backscatter). The radar data agreed to within 3 dB with a buoy measurement of the omnidirectional spectrum at the Bragg resonant frequency, 0.14 Hz.

One can write the ocean wave directional power spectrum as:

$$S(\vec{K}) = S(K,\theta) = S(K)\, F(\theta),\tag{4}$$

where the approximation has been made that the angular dependence of the spreading of ocean waves is independent of wave number. The first term is the so-called omnidirectional energy spectrum, since $F(\theta)$ integrated over all angles gives unity. A typical form for the omnidirectional spectrum is the Pierson-Moskowitz spectrum, [5]:

$$S(\Omega)\, d\Omega = \alpha g^2\, \Omega^{-5} \exp\left(-b\,(g/\Omega w)^4\right)\, d\Omega\tag{5a}$$

or, in terms of wave number,

$$S(K)\, dK = (\alpha/2)\, K^{-4} \exp\left(-b\,(g/Kw^2)^2\right)\, dK,\tag{5b}$$

where w is the wind speed at 19.4 ft above the sea surface; b is a constant, 0.74; Ω is the wave frequency in radians; and α is typically of the order of 0.0081 for long fetches, as proposed by Phillips, but which has been shown to be a function of fetch. (See, for example, Hasslemann et al., [6].) A plot of a series of ocean wave spectra is shown in Fig. 1 as a function of wind speed generating the seas, and also for two values of the variable, α. The effect of changing α is to raise or lower the asymptotic Ω^{-5} line.
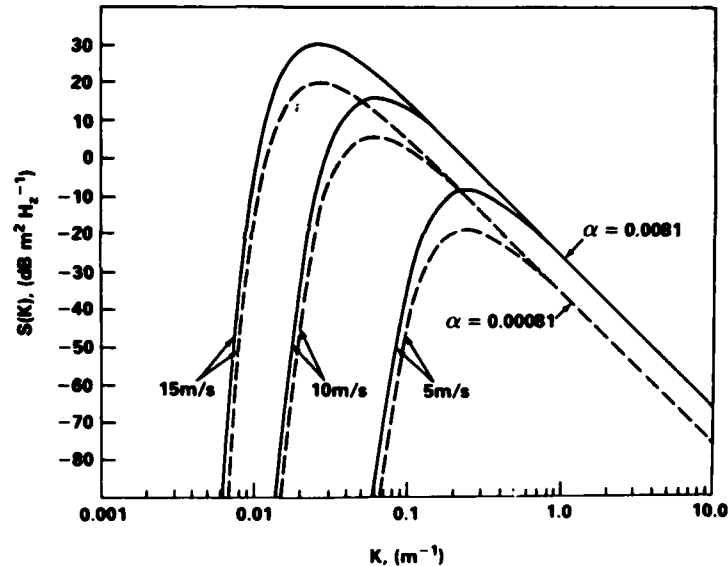

Fig. 1 — Two families of curves representing ocean wave spectra given by Eq. (5b) in the text are shown. Each family is parametric in the wind speed, with the low frequency amplitudes growing with the wind. The difference between the two families is the constant, α, the upper family determined using a value of 0.0081, while the lower family is determined by an α of 0.00081. The decibel difference between the two asymptotes at the high frequency end is seen to be ten dB as a result of the factor of ten decrease in α.

Since the radar cross section is determined essentially by the sum of the first-order contributions to the Doppler spectrum, and these terms are proportional to the amplitude of the ocean wave spectrum at the Bragg wavelength, the radar cross section will vary linearly with the parameter α:

$$\sigma^0(\theta,\omega_D) \approx 4\pi\, \alpha\; \left(F(\theta)\,\delta(\omega_D + \omega_B) + F(\theta + \pi)\,\delta(\omega_D - \omega_B)\right).\tag{6}$$

In the above we have set the exponential factor of Eq. (5b) to one, since it affects the spectrum near the low frequency falloff, but not near K_B (5 to 15-m ocean wavelengths).

3

When operating in a normal monostatic mode, if one steers a very narrow beam radar operating line of sight or in the surface wave mode, one will observe the maximum Bragg line of the approach-recede pair to reach its maximum amplitude in the direction that is parallel to the wind. The weaker of the two will likewise reach its minimum value at this bearing. The ratio of the two, ρ, will thereby reach its maximum value. At right angles to the wind direction, this decibel ratio goes to zero, as the maximum Bragg peak has decreased and the minimum has increased such that the two are equal. This behavior with angle reflects the fact that the variations in ρ are strictly due to the variation of the spreading function of Eq. (4) with angle. Since the omnidirectional spectrum is the same over the area covered by the radar (very short ranges are assumed), the only variation in the left hand side of Eq. (4) is due to $F(\theta)$. Given a model for the spreading function, one can use this technique to estimate the angle that the radar bearing makes with the wind driven waves for a single radar bearing. This technique has been implemented in the skywave mode of operation to derive wind direction fields over large expanses of the ocean [7] and to locate hurricane centers and define fronts using very narrow beam antennas [8].

Although this technique allows the estimation of direction, the problem of estimating the first term of Eq. (4) from first-order Bragg line measurements used with the radar equation alone remains difficult because of the antenna gain uncertainties. Additional information is available in the second-order contribution, however, which can allow one to estimate the amplitude of the parameter, α, and, hence, allow a similar estimation of σ^0. First, an introduction into the second-order contribution to the Doppler spectrum is necessary.

SECOND-ORDER BRAGG SCATTER

In the following, we shall give an intuitive development of the simple corner reflector model used to describe second-order scatter. This is the basis of the work by Trizna et al. [9] and differs from work by Barrick [10], who has considered both electromagnetic and hydrodynamic contributions to the second-order structure of the radar Doppler spectrum. Valenzuela [11] has considered both of these contributions as well, but his results are more general, since they were derived for microwave frequencies, and are valid at the long wavelength limit appropriate to HF frequencies. The hydrodynamic resonant term of Valenzuela differs from that of Barrick in that it contains a viscous damping term, ν, which is very important for the microwave radar frequencies examined in detail by Valenzuela, and possibly in the HF regime as well. This point is an area of current investigation. A rigorous development of the corner reflector model is in preparation for publication, and begins with the integral equation for the second-order contribution to the scattering cross section developed by Valenzuela (Trizna, in preparation).

Basic Physical Assumptions for Second-Order Scatter

For the second-order electromagnetic contribution, which is the major term near zero Doppler for all cases, we use the corner reflector model as outlined in Trizna et al. [9]. The electromagnetic wave scatters twice from all possible pair combinations of ocean waves that are travelling perpendicular to one another. Each individual pair produces a response at a different point in the Doppler spectrum which is determined by the Doppler shifts produced by each wave travelling at its appropriate phase velocity. The electromagnetic resonance term of Barrick allows all possible combinations of ocean wave vectors to contribute in double scatter, without the restriction that the wave pairs be perpendicular to one another. Instead, he considers the first wave as arbitrary to begin with, as we do, then considers all possible ocean waves for the second scattered radar wave, using a factor, Γ, which is resonant for the case when the second wave is perpendicular to the first. In effect, the difference between the two techniques is that he considers Γ as a resonance with some shape, whereas we, in effect, evaluate it as a δ-function when performing the integration.

4

The problem of radio scatter from physical ocean waves is considered in the same sense as one would consider radio scatter from any physical object, with regard to the calcula'ion of the phase shifts produced by the nonzero velocity of the object. Two laws of physics can be used as starting points for setting up the calculation, namely, the law of conservation of momentum, and the law of conservation of energy. It is to be noted that these are in fact laws of physics which have been verified and used in classical mechanics and electromagnetism, as well as quantum physics and special and general relativity. They are starting points, for example, for the calculation of the relativistic interaction of photons with matter, and degenerate to our problem in the classical limit (See, for example, Leighton [12], Ch. 1).

Double Scatter Wave Numbers—Conservation of Momentum

If one first invokes the law of conservation of momentum for the scatter, then the following equation results for the total momentum conserved for the double scatter of the electromagnetic wave from two ocean waves with wavenumbers, $\vec{K}_1$ and $\vec{K}_2$:

$$h \vec{K}_1 + h \vec{K}_2 = 2 h \vec{k}, \tag{7}$$

which is a vector equation, where 'h' is Planck's constant. The scatter can be divided into two independent scatters, with an intermediate electromagnetic wave, with wavenumber, k'. Momentum must be conserved in this intermediate scatter as well ([13], p. 145). The resulting equation describing the first scatter is given by:

$$h \vec{k} = h \vec{K}_1 + h \vec{k}'. \tag{8a}$$

If one solves the above equation in component form, one sees that the intermediate scatter must reflect from the first ocean wave at an angle to the first wave number vector equal and opposite to the incident angle. One can now consider the second scatter, with the incident wave now the intermediate wave, k'. A similar equation results, namely:

$$h \vec{k}' = h \vec{K}_2 + h \vec{k}''. \tag{8b}$$

For the radar energy to scatter back to the radar, k'' must be in the opposite direction as k, so

$$\tilde{k}'' = - \tilde{k}, \tag{9}$$

where the $\tilde{\ }$ denotes the unit vector defining the direction for each wave vector. Solving Eq. (8b) in component form again requires the scattered angle be equal to the incident angle. The choice of the direction defined by Eq. (9), when combined with (8a) and (8b), sets the direction of K_2 as perpendicular to K_1, as is shown in Fig. 2. That is, because conservation of momentum demands that radar waves scatter specularly from ocean waves in the plane of the ocean surface, choosing the final scatter direction to be back to the radar requires the two ocean waves participating in the scatter to be perpendicular to one another. Instead of this intuitive development using the intermediate scatter concept, Eq. (7) can be used alone, in conjunction with the integral equation for $\sigma_{(2)}^0$ (ω_B, θ), as a delta function, to derive the closed form for $\sigma_{(2)}^0$ (ω_D, θ) for a perfectly conducting sea surface. This mathematical development does not assume that the intermediate scatter be specular in the plane of the sea surface, but it follows as a result of the development.

Doppler Shift Calculation—Conservation of Energy

For a given pair of ocean waves satisfying Eq. (7), the amount of Doppler shift from the transmitted frequency is determined by the conservation of energy equation:

$$\hbar s_1 \Omega_1 + \hbar s_2 \Omega_2 = \hbar \omega_D, \tag{10}$$

where $\hbar = h/2\pi$ and where ω_D is the Doppler shift of the received radar energy scattered via ocean waves 1 and 2. Note that there are more than one pair of ocean wave frequencies which can satisfy Eq. (10) and all such pairs must be considered.
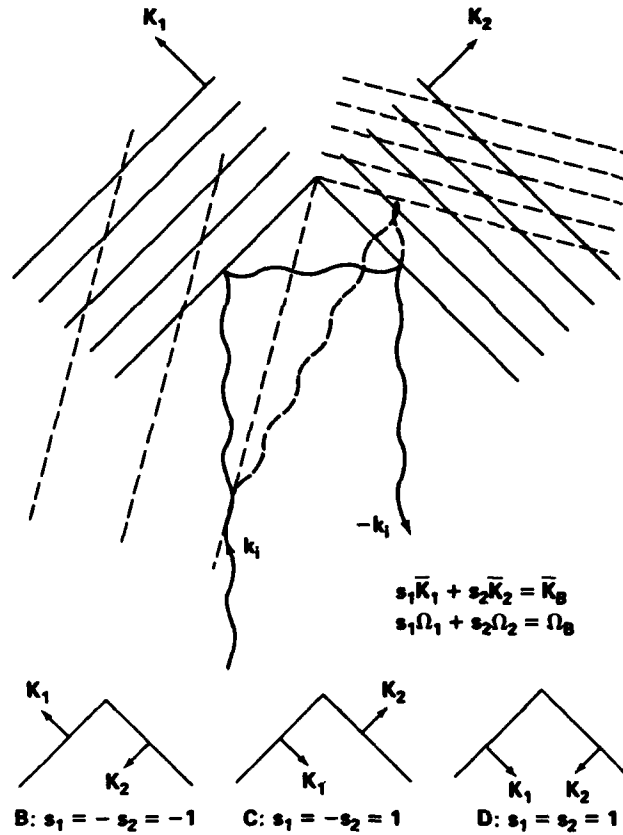
Fig. 2 — The double scatter mechanism responsible for second order
Doppler structure is shown by a plan view as seen from above the
surface. Four possible combinations are indicated for one value of
the angle between $\overline{K}_1$ and $\overline{k}$, $\Theta = 45$ deg, with cases B and C giving
a zero Doppler contribution. Cases A and D will contribute at
$\pm 2^{3/4} f_B$, respectively. A case for a second value of Θ is shown in
dashed lines, with different wavelengths for K_1 and K_2, yielding a
different Doppler shift.

Determination of the Scattered Energy per Doppler Filter

The calculation of expected energy per Doppler filter is carried out in a systematic manner, run-
ning through the combination of wave vectors, $\overline{K}_1$ and $\overline{K}_2$, which satisfy Eq. (7). One begins with the
magnitude of K_1 very nearly zero, and K_2 very nearly equal to the Bragg wave number, K_B. The
angles that the two wave vectors make relative to the incident electromagnetic wave vector are required
to satisfy the vector equation of Eq. (7), in component form along arbitrarily chosen orthogonal axes,
say the y-axis along the incident electromagnetic wave vector in Fig. 2. The corresponding ocean wave
frequencies are determined using the dispersion relation for linear gravity waves relating K_B and Ω_B,
given just after Eq. (3). The Doppler frequency at which this contribution appears in the Doppler spec-
trum is then given by Eq. (10). At each Doppler spectral point, for a given Doppler filter width, there
is a corresponding spread in angle and wave number dK_1 and dK_2, which contribute to the Doppler
filter considered. For a specified look angle of the radar relative to the wind direction, the amplitude
contribution at each Doppler spectral point is then determined by integrating the expression for the

6

second-order scattering coefficient, $\sigma^0_{(2)}$, over Doppler frequency with an appropriate Doppler filter shape to determine the scattered energy within the given Doppler filter:

$$\sigma^0_{(2)}(\omega_D, \theta) = 2^6 \pi k^4 \int d\omega'_D \int d\overline{K}_1 \ |\Gamma|^2 \ S(\overline{K}_1) \ S(\overline{K}_2) \ G(\omega_D - \omega'_D) \ \delta(\omega'_D \pm \Omega_1 \pm \Omega_2), \quad (11)$$

where Γ is given in [10,11], and $G(\omega_D - \omega'_D)$ represents the spectral response of the FFT filter, typically a sinc-function if no time weighting is done on the FFT. This integral is further considered in a future publication (Trizna, in preparation), but the results are essentially the same as in [9].

Note that the first-order Bragg line energy is obtained in a similar manner, integrating Eq. (6) over Doppler frequency with an appropriate Doppler filter shape. Note also that the first- and second-order contributions behave differently with different coherent integration times, or Doppler filter line widths. Because the first-order Bragg line is a coherent discrete spectral line return with fixed total energy, the response will increase relative to the noise level with narrowing Doppler filter width. However, the second-order term is a noise-like continuum, and as the Doppler filter is narrowed, a smaller spread in dK_1 and dK_2 is included for a given Doppler filter, as discussed above. This excluded energy appears in an adjoining Doppler filter, and as such, behaves as a noise spectrum rather than a coherent narrow spectral return. (As the coherent integration time is doubled in the FFT process and the spectral width of the FFT filter is halved, the number of spectral filters is doubled across the total Doppler bandwidth.) The details of this discussion will be covered in the future publication cited above.

TECHNIQUE OF σ^0 DETERMINATION

The determination of σ^0 depends upon two measurements, that of the ratio of approach/recede Bragg line amplitudes, ρ, and a measure of the amplitude ratio of maximum Bragg line to zero Doppler continuum, ζ, plus a consideration of the coherent integration time used in the processing. The first measurement allows one to determine the angle to wind/wave direction the radar bearing makes, and thereby allows a determination of $F(\theta)$ in Eq. (3). The second measurement allows a determination of the Phillips' constant, α, of Eq. (5), using Eqs. (6) and (11) for zero Doppler frequency. With knowledge of α and θ the radar cross section is thereby determined using these in Eq. (6). A final correction is also made for the integration time, or Doppler filter width used, and is included in the final results.

Figure 3 shows two spectra, illustrating the effect of a different value of α. For the same wind speed, but a 10 dB decrease in α (vis-a-vis Fig. 1), the Doppler spectrum frequency characteristics remain quite similar, except for a 10 dB decrease in the first-order Bragg lines, and a 20 dB decrease in the second-order continuum amplitude. This is what one would expect for once- and twice-scattered radar waves, each scatter being proportional to a resonant ocean wave component, vis-a-vis Eqs. (3) and (11).

Determination of the Relevant Ocean Wave Components

The relationship between measured ζ and the resulting Phillips constant, α, requires knowledge of which components are being sensed by the radar at zero Doppler. From Eq. (10), the Doppler frequency is zero for the corner reflector case of the magnitudes of the two ocean wave frequencies being equal, which requires that the magnitude of the corresponding wave numbers also be equal. In addition, if one writes Eq. (7) in component form, in a set of coordinates discussed earlier, one has:

$$s_1 K_1 \cos \Theta + s_2 K_2 \sin \Theta = 2k \quad (12a)$$

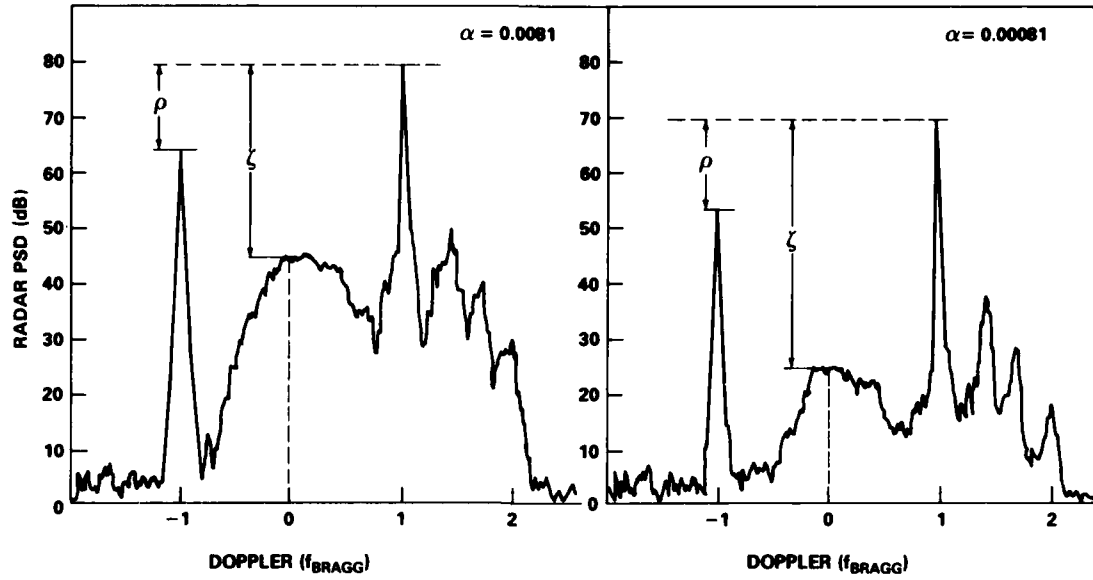$$s_1 K_1 \sin \Theta - s_2 K_2 \cos \Theta = 0 \quad (12b)$$

Fig. 3 — Two different radar Doppler spectra illustrate the effect of changing the constant α of Eq. (4) by a factor of ten, due to the sea surface being 10 dB down from traditional saturation values in the high frequency regime. The first-order Bragg lines are down 10 dB and the second-order continuum is down 20 dB, ten more than the first order, in the second spectrum compared to the first. These might be the result of wave spectra from Fig. 1, for the same wind speed and the two α's differing by a factor of ten.

where Θ is the angle between K_1 and the x-axis, and s_1 and s_2 are arbitrarily chosen as $+$ or -1. The region between the Bragg lines filled when s_1 and s_2 are chosen with opposite signs, and to the right/left of the Bragg lines when both are positive/negative. The only Θ which satisfies Eq. (12b) for $K_1 = K_2$ and $s_1 = -s_2$ is $\Theta = 45°$. From Eq. (10), for zero ω_D, $\Omega_1 = \Omega_2$, and hence, $K_1 = K_2$ for $s_1 = -s_2$. Substituting this value into Eq. (12a) then gives the magnitude of

$$K_1 = K_2 = k/(\sin 45°) = \sqrt{2} \, k. \tag{13}$$

The corresponding ocean wave frequency (using the gravity wave dispersion relation, $\Omega = \sqrt{gK}$, and $K_B = 2 \, k$) responsible for scattered energy as zero Doppler frequency is found to be:

$$\Omega_0 = \Omega_1 = \Omega_B/2^{1/4} \tag{14}$$

$$= 0.841 \, \Omega_B.$$

Hence, the ocean wave frequency sensed by the second-order Doppler energy at zero Doppler frequency is very nearly the same as the wave frequency sensed by the first-order Bragg scatter, and is generally far from the peak of the spectrum, but almost certainly in the region where the wave frequency spectrum behaves as Ω^{-5}. The directions of propagation of the two components, such that the net Doppler frequency is zero, is determined to be $45°$ to the right and left, respectively, of the radar pointing direction, with one ocean wave approaching and the other receding from the radar. (Note that there are two such pairs, cases A and D of Fig. 2, and both are taken account of in the radar spectrum model.) In the model used for determination of $\sigma_{(2)}^0(\omega_D)$, the assumption is made that the ocean wave power spectrum does vary as Ω^{-5} near the Bragg wave frequency in amplitude, with the angular dependence of Eq. (4) varying as:

$$F(\Theta) = \frac{2}{\pi} \, (a + \cos^2 \theta), \text{ for } 0 < |\theta| < \pi/2 \tag{15}$$

$$F(\theta) = 2a^2/\pi \, (a + \cos^2 \theta)^{-1}, \quad \text{for } \pi/2 < |\theta| < \pi.$$
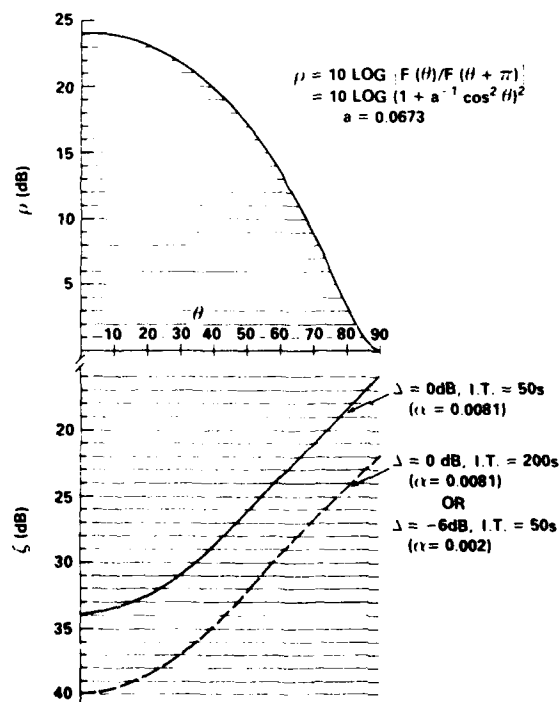
8

(See [7] for a further description of this model.) Because the wave number determined by Eq. (13) is very close to the Bragg wave number, the error in the Ω^{-5} assumption is minimal. A greater error is probably present due to the assumption of the angular spreading used. We shall discuss this in a later section.

Since the Bragg ocean wave frequency, Ω_B, and the wave frequency contributing to the zero Doppler amplitude, Ω_0, are nearly equal from Eq. (14), both are unaffected by the exponential of Eq. (5) and will scale in a similar manner with changing α. That is, as long as the peak of the wave spectrum is much less than the Bragg ocean wave frequency, slight changes in the position of the peak due to different wind speeds will have no effect on the wave spectrum amplitude at Ω_B and Ω_0. The amplitude at these frequencies will be determined only by the parameter, α, (which is a function of fetch) and wind/radar angle, Φ_{WR}, so long as the wind is sufficiently strong to drive the peak of the spectrum far from the Bragg frequency, so that the exponential term of Eq. (5) is nearly one.

Results in Nomograph Form

The model for the Doppler spectrum by [9] was used to generate curves of ζ, the ratio between the strongest Bragg line in the Doppler spectrum, and the zero-Doppler continuum amplitude, for various values of the parameter, α. The results are shown in Fig. 4, in the form of a nomograph. The horizontal axis is wind to radar angle. The positive y-axis is ρ, the ratio of approach to recede Bragg line power. The negative y-axis is the parameter, ζ, the ratio of the maximum Bragg line power to the power level of the zero-Doppler continuum, which is a function of wind-radar angle. The curve in the lower half plane labeled with Δ equal to zero is the locus of ζ for a value of the constant, α, equal to 0.0081, historically taken as the Phillips "saturation" value for the constant α, and a coherent integration time of 200 s.

Fig. 4 — A nomograph derived from theoretical spectra that allows one to calculate the number of dB, Δ, the ocean wave Bragg wavenumber (and σ^0) is down from the Phillips saturation value, .0081 (used only for a reference value). With the measured value of ρ, the approach-recede Bragg line ratio, one determines the angle to wind of the radar bearing, θ, using the upper half plane. Measuring ζ, the ratio of largest Bragg line to zero Doppler second order amplitude, one draws a horizontal line. The point at which this horizontal line intersects the vertical line drawn down from the estimated radar-wind angle, θ, determines Δ, the number of dB the point is down from the theoretical curve for the specified integration time. This value is then used in Eq. 21 of the text to determine $\sigma^0(\theta)$.

$\rho = 10 \, \text{LOG} \, [F(\theta)/F(\theta + \pi)]$
$= 10 \, \text{LOG} \, (1 + a^{-1} \cos^2 \theta)^2$
$a = 0.0673$

$\Delta = 0\text{dB}, \text{I.T.} = 50\text{s}$
$(\alpha = 0.0081)$

$\Delta = 0 \text{ dB}, \text{I.T.} = 200\text{s}$
$(\alpha = 0.0081)$
OR
$\Delta = -6\text{dB}, \text{I.T.} = 50\text{s}$
$(\alpha = 0.002)$

9

If the omnidirectional sea spectrum is down 6 dB from this value, then the first-order Bragg line amplitudes will also be down 6 dB each from their "saturated" values. The ratio of the Bragg lines will not be different, however, since they depend only upon the directional factor of Eq. (3). Since the zero-Doppler amplitude is of second order in the ocean wave spectrum, it will be down 12 dB from its value for the "saturated" sea. The ratio ζ will decrease by the difference in the dB change of the first-order Bragg line and the second-order zero-Doppler continuum, i.e., 6 dB. A second curve is shown in the figure, just 6 dB below the first with the same variation with angle. The value of α corresponding to this curve is therefore 0.0020 for the same integration time as the first curve. This second curve can also be considered as derived for α equal to 0.0081, but for an integration time four times less than for the first curve, as indicated in the figure, 50 s. (This is of course due to the fact that the Bragg line is a coherent signal, while the continuum is broadband and hence behaves as noise. They sum like T and $\sqrt{T}$, respectively, where T is the coherent integration time.)

To use the curves, one takes the measurement of ρ, draws a horizontal line until it intersects the curve in the upper half plane, and determines a radar-wind angle by dropping a perpendicular from this intersection to the x-axis. One continues this vertical line into the lower half plane. One then takes the value of ζ measured from the radar spectrum which gave ρ, and draws a horizontal line until it intersects the vertical line drawn earlier. The number of dB this intersection lies below the theoretical curve is Δ, the number of dB down the scattering cross section of the sea is from its saturated value for that radar wind angle. This value must yet be corrected for the integration period one used in processing the radar Doppler spectrum that produced ρ and ζ. Since the curves were generated for a 200 s integration time, if the integration time used is half this value, 3 dB should be added to Δ; if quadrupled, 6 dB is added, and so on. In the case of ionospherically propagated signals, particularly via F-layer modes, one should either choose an integration time such that the Bragg lines just fill the Doppler filter, or sum up the energy in all the Doppler filters which have contributions from the Bragg line for longer integration times. The simplest course is to use 50-s integration times, which have been found optimum for very good ionospheric conditions, and use the 50-s curve in the figure. If the ionospheric conditions are relatively poor with a 50-s value, so that the Bragg line contributes to several adjacent Doppler filters, then one must sum all of the energy in the Bragg lines, possibly encompassing several Doppler filters in calculating ζ. This is not important in determining ρ, since both Bragg lines are affected the same way, but must be done in measuring ζ. These effects are discussed in greater detail in the next section.

EFFECTS OF INTEGRATION TIME, RADAR SIGNAL BANDWIDTH, AND EFFECTIVE BANDWIDTH DUE TO DEGRADATION OF SEA SURFACE AND IONOSPHERIC COHERENCE

There are several limits that prevent one from achieving an infinitely narrow Bragg line width as one increases the coherent integration time indefinitely. Barrick indicated in his work that the Bragg line has zero width and infinite amplitude, but that the product of the two is a finite value. However, he did not consider the fact that one transmits a finite bandwidth, scatters from finite patch sizes on the sea surface, and is affected by coherence lengths within the ionosphere. (His calculation assumed an infinite plane wave upon a perfectly coherent and infinite surface.) We consider each of these in increasing order of importance in this section.

Doppler processing of coherent radar data is equivalent to matched filtering, so that the response from the filter has a finite width. In terms of the FFT, each spectral point has a finite width equal to the total FFT bandwidth, which is equal to the pulse repetition frequency (assuming sum and quadrature FFT inputs), divided by the number of FFT input points. If the backscatter is indeed infinitely narrow inherently, the measured spectrum will equivalently be $1/T$ Hz wide, where T is the coherent integration time used. (Doubling the coherent integration time, or input points to an FFT, is equivalent to halving the bandwidth of the matched filters and doubling their number.) As the integration time is increased indefinitely, the spectrum would not decrease indefinitely for a pulsed signal of

10

bandwidth, W, but would reach a minimum width, δF_{min1} as determined by the transmitted bandwidth to radar frequency ratio:

$$\delta F_{min1}/F_{Bragg} = \delta F_{BW}/F_{Radar} \tag{16}$$

where F_{Bragg} is the Doppler frequency of the Bragg line; δF_{BW} is the transmit bandwidth used; and F_{Radar} is the radar operating frequency. For a 100-μs pulse (10-kHz bandwidth), and a 10-MHz radar frequency, the ratio of the above equation is 0.001. For this case, the minimum line width one can achieve by increasing integration time is 0.001 times the Bragg line Doppler shift, or 0.00314 Hz, where f_B (Hz) $\approx 0.102\sqrt{f_{radar} \text{ (MHz)}}$ relates the radar frequency and the Bragg line Doppler shift. Narrowing the bandwidth to 100 kHz using a 10-μs pulse, would result in just a 0.0314-Hz minimum achievable Bragg line width. Further increases in the integration time beyond this minimum simply creates more Doppler filters, narrower in bandwidth, the sum of which maintain the shape of this minimum width Bragg line signal. This is the minimum one should achieve if the scattering surface were perfectly coherent over the entire radar cell (scatter from a land surface, for example) and if the ionosphere were a perfectly coherent reflector. However, earlier width limitations are reached, which are broader than F_{min1}.

One earlier limitation to minimum achievable line width is determined by patch size effects on the ocean surface. That is, the scattering surface is not coherent over the radar pulse length. This is primarily due to the fact that the ocean wave spectrum is not a linear one, but does exchange energy between components. To first order, the Fourier approximation holds, since the time of transfer of energy is long compared to most measurements of a given component. As one increases the integration time on processing, one reaches times of the order of energy exchange processes within the wave spectrum. The waves are behaving as wave packets, equivalently, with spatial extent smaller than the radar pulse. Now the minimum linewidth one can achieve for a given Bragg line is no longer related to the reciprocal of the pulse length, but to the reciprocal of the size of the wave packets on the ocean surface. Although this effect has not been investigated in detail, typical values of 100 to 200 s are the limitations imposed by wave packet size effects to the integration times one can use before the Bragg line ceases to narrow.

The most severe linewidth limitation is provided by the ionosphere. Propagation through the magneto-ionic medium and refraction back to earth results in phase changes which may not be uniform across the phase front of the radar wave. If one thinks of the refraction as a reflection from a virtual surface at some virtual height, which produces the equivalent final wave vector, one can again think in terms of coherent areas on this virtual surface. These areas are due to ionospheric turbulence, and cause time rates of change of phase paths of refracted radar signals. For F-layer propagation the size of these patches is typically less than those on the ocean surface, and the maximum useful integration times available are typically 25 s, although more stable conditions are often encountered. Propagation via the E-layer is generally much better, and quite often the sea surface is the limiting factor in determining minimum achievable line widths. Integration times of up to 100 s have been used successively via stable E-layer propagation.

The net effect of this section on our point of interest is that one must consider the total energy within the broadened Doppler Bragg line as the measurable quantity for the determination of both ρ and ζ. In either the case of the sea surface or the ionosphere, where patch size effects dominate, scatter from the various patches have some distribution which is Gaussian regarding the sum phase of scatter from all of the resonant patches. In processing radar data for these cases one should attempt to match the integration time used to the bandwidth limiting the linewidth so that the peaks of the Bragg lines are a good representation for the energy within the Bragg line, i.e., so that all of the appropriate energy in a Bragg line is contained in a single Doppler filter. Then one can simply scale peaks in measuring ζ, and no additional corrections for integration times or linewidth effects are necessary. If longer integration times are used than this "matched" one, one must sum up the energy in all the Doppler filters which contain significant contributions to the Bragg line. Shorter integration times than the matched one may

11

be used with little effect, as long as second-order scatter, sufficiently far from zero Doppler so that Eq. (14) is poorly satisfied, does not fall within the zero Doppler filter, affecting the measure of ζ.

An example of the effect the coherence of the ionosphere has on minimum achievable linewidth is shown in Fig. 5. A total time period of 409.6 s of radar data was processed with several integration times, then incoherently averaged so that the same data period is covered in each case. For the transition from 25.6 to 51.2 s occurs, the expected line narrowing occurs, and a 3 dB increase of the Bragg peak relative to the continuum second-order occurs. This second-order scatter, which is broadband, will fill all Doppler bins between the Bragg lines irrespective of the coherent integration time used here. As the coherent time is increased from 51.2 to 102.4 s, the effects of the ionosphere begin to appear, the line does not narrow by a half as expected, nor is there any increase in the ratio of Bragg line peak to zero Doppler energy. In both cases now the scattered energy has a finite inherent line width imposed by the ionosphere. Further increases in integration time will simply fill additional Doppler bins with scattered energy, with no change in amplitude or improvement in signal to noise. The signal has in effect become noise-like in the sense that it is spread over a finite bandwidth and cannot be further spectrally isolated by increasing integration time. The final change from 102.4 to 204.8 s again causes no change in the ratio of Bragg peak to zero Doppler continuum level, although the Bragg lines are decomposed more clearly into the various ionospheric multipath contributions.

σ^0 DEPENDENCE ON SPREADING FUNCTION USED

Determination of $\sigma^0_{(1)}$ is affected in two major ways by the spreading function one uses to define the directional sea spectrum. First, the value of ρ is determined by the ratio of amplitudes of the directional wave spectrum at an angle parallel to the direction of the radar look divided by the amplitude π radians to that direction, $F(\theta)/F(\theta + \pi)$. Second, the amplitude of σ^0 along the wind direction will vary in an absolute sense for different angular spreading models, and these are known to differ greatly for early periods of wave growth, when the wave energy is highly peaked along the wind direction, versus later periods when the wave energy has spread in angle. (See, for example, [14].) In addition to this fixed frequency behavior with time, angular spreading is observed to vary with wave frequency for a given time in the wave development process as well. As a result of this type of behavior, a directional spectrum highly peaked along the wind direction, compared to a spectrum generally uniformly distributed in angle, can give the same integrated result for a given frequency component when measured by an omnidirectional instrument such as a Waverider buoy. However, a radar measurement will yield a greater angular spectral power value for a look angle along the wind direction in the case of the highly peaked spectrum than for the spread spectrum, since it is measuring just a small angular portion of the ocean wave directional spectrum rather than the integrated value over all angles as is done by a buoy. The value of ρ measured will differ for the two cases as well, and can give incorrect results in use of the nomograph if the sea spectrum does not spread as given by Eq. (15). However, for open ocean conditions and far from the spectrum peak in frequency, Eq. (15) can be considered as valid.

Concerning the second point, Barrick's original paper defining σ^0 as -29 dB was developed using an omnidirectional wave spectrum with equal amplitudes in all directions in the forward half plane, with no energy in the back half plane opposite the wind, and with a constant α of 0.01 in Eq. (4). For this case, ρ could not be defined because a weaker Bragg line does not exist. If one sets a back plane energy level some constant value, some number of dB down from the forward plane energy, the value of ρ remains constant with look angle, which observationally is not true. If one allows some directionality to the spreading function, then the amplitude of the radar cross section must increase along the wind direction compared to the -29 dB predicted by Barrick, such that the integrated wave energy over all directions is the same for any directional spreading function.
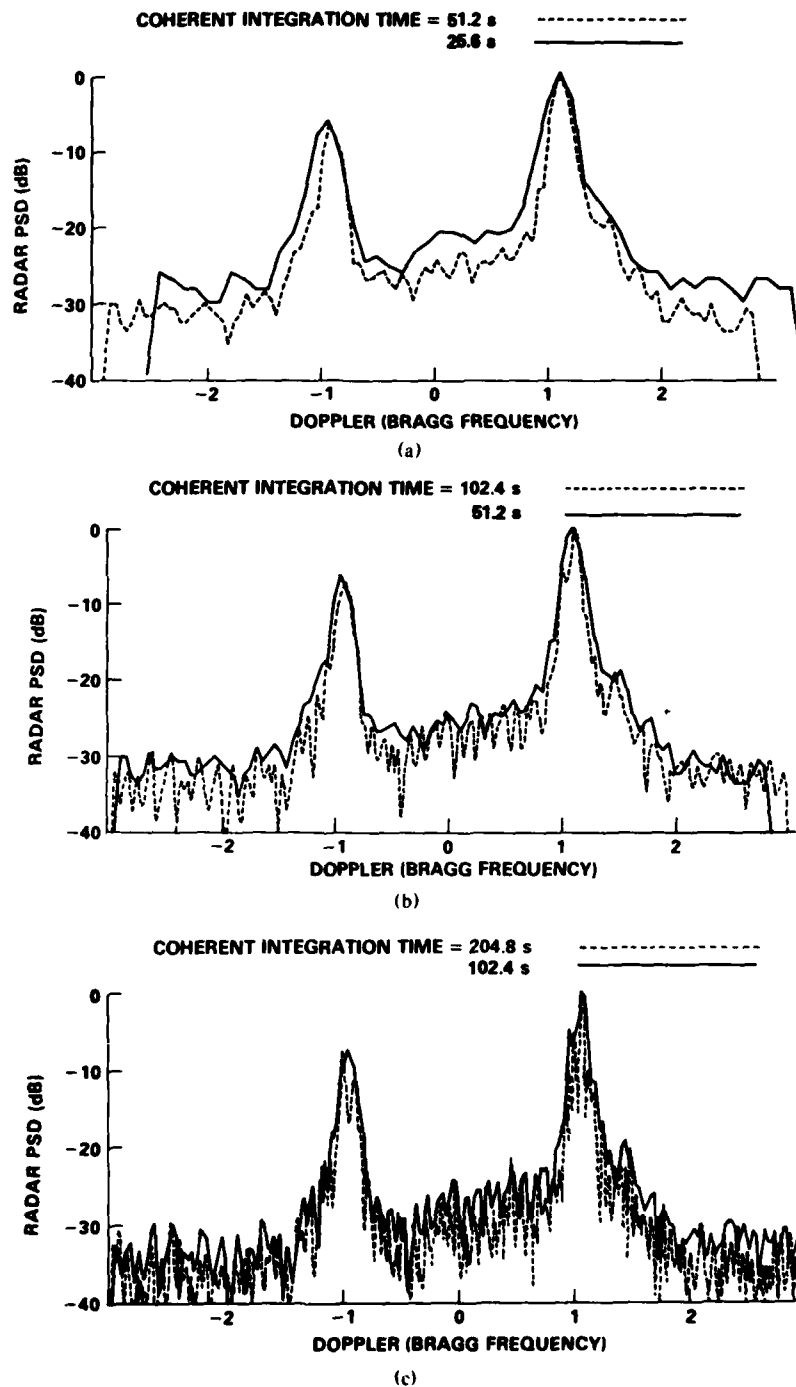
12

Fig. 5 — The same period of radar data, 409.6 s, was processed using four different integration times, with spectra incoherently added to cover an identical time period for skywave propagation. With the change from 25.6 to 51.2 s (5a), narrowing of the Bragg lines and the expected 3 dB increase in ζ is observed, as described in the text. With a further increase to 102.4 (5b) and 204.8 s (5c), ionospheric multipath prevents further Bragg line narrowing, and no change in ζ, as described in the section on effects of integration time, etc.

13

Figure 6 illustrates this fact by a plot of σ^0 as a function of angle to the wind for a selection of models of directional spreading functions, using Phillips' value of 0.0081 for α in place of Barrick's 0.01. The corresponding constant value of -29.9 is the smallest value of the set along the wind direction, while the largest value in this direction is given by the most highly peaked spreading function. In all cases, the integrated energy under each curve over all angles is the same, as is necessary from the discussion in conjunction with Eq. (3).
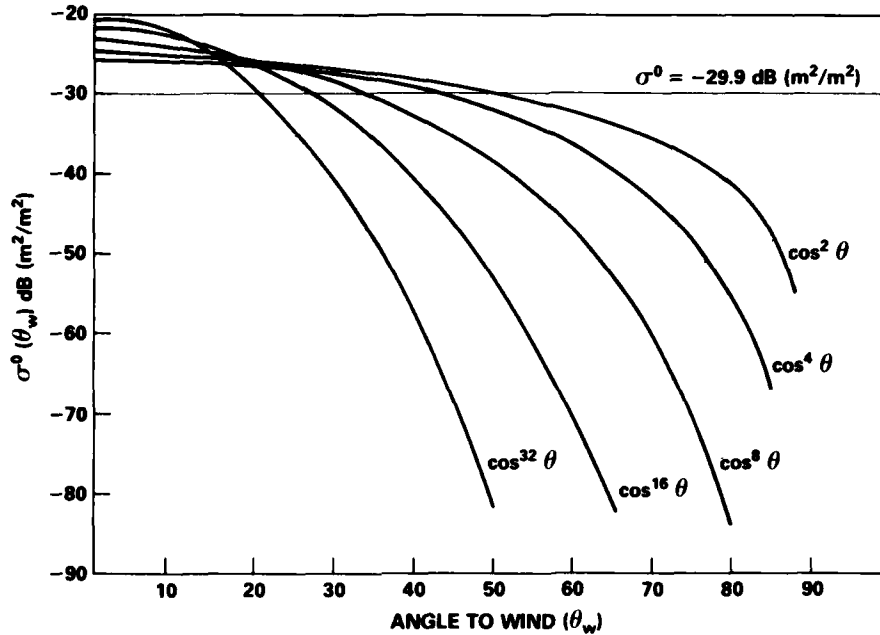

Fig. 6 — Curves of σ^0 for "saturated" sea spectra are shown as a function of radar-wind angle for different models of the directional spreading function, $F(\theta)$, of Eqs. (3) and (4) in the text. The straight line is Barrick's result, slightly modified for a Phillips constant of 0.0081 rather than 0.005 used by Barrick [3]. It is seen that as energy is localized about the forward direction relative to the omnidirectional model, the cross section along the wind direction must rise compared to the constant value of -29.9 dB. This normalization comes about because the integrated area over all angles under the curve must give the same result, corresponding to the energy measured by an omnidirectional wave measuring device which does not distinguish angular information, and for which the Phillips, Pierson-Moskowitz, and other wave models are defined.

The spreading function used will affect the determination of σ^0 in one additional way, via its use in calculating $\sigma^0_{(2)}$ and derivation of the nomograph. The double scatter mechanism used to calculate the second-order contribution at zero Doppler frequency depends upon this spreading, but the magnitude of this effect has not been investigated. An example of the variation in the angular spreading of two models is shown in Fig. 7, where we have plotted the spreading function:

$$\pi^{-1} F(\theta) = \beta + \cos^2\theta, \quad \text{for } |\theta| < \pi/2 \tag{17a}$$

$$\pi^{-1} F(\theta) = \beta^2/F(\theta + \pi), \quad \text{for } |\theta| > \pi/2 \tag{17b}$$

as well as an example of another popular model given by:

$$\pi^{-1} F(\theta) = \beta + \cos^s (\theta/2). \tag{18}$$

Constants β were chosen for both models so that the front to back ratio are both 24 dB. The exponent, s, of the second model was then chosen such that both models had the same value at 90° to the wind direction as well. It is noted that there are no more than a few dB variation over all angles, and that
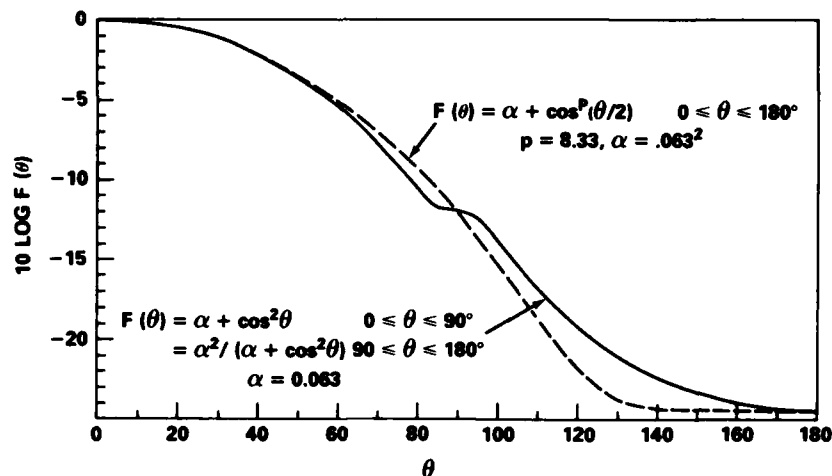
Fig. 7 — Plots of the spreading function, $F(\theta)$, of Eqs. (17) and (18) of the text are shown plotted as a function of angle to wind. The solid curve is the model used in Trizna, et al. [9] whereas the dashed curve is of a type determined from pitch and roll buoy analyses. Constants have been chosen for this model so that both models have the same upwind-downwind ratio, 24 dB, as well as equal amplitudes at 90°. Both are empirical and neither has been derived from first principles. The point to note is that both models can be mapped into the other with just a few dB of difference over all angles. The dashed curve used to generate radar spectra and the nomograph would probably produce results similar to the solid curve.

both models are virtually identical out to 60° from the wind direction. It is not expected that the nomographs generated using these two models would differ significantly from one another, although use of a much more peaked spectrum would produce different results. Additional work in this area, using frequency dependent spreading functions, is ongoing. Indeed, accurate representation of the spreading of wave energy as a function of wave frequency is one of the biggest uncertainties faced in modeling second-order radar Doppler spectra.

EXAMPLES OF RADAR DATA COMPARISONS
WITH WAVERIDER BUOY RECORDS

The technique of determining σ^0 from radar data using the nomograph was applied to surface wave data collected at San Clemente Island using a radar with a 15° beamwidth that is constant with radar frequency, made so by selectively omitting elements with increasing radar frequency. The radar was run at ten frequencies and two bearings separated by 30°, switching frequencies and then bearings on a pulse-to-pulse basis, so that in effect the data were collected simultaneously. The radar spectra were processed with a 200-s integration time, that for which the nomograph was developed so that no correction is required for the integration time. The ten frequencies used run from slightly above 2 MHz to 24 MHz. Data were collected for three range bins, sampled time delays of 50, 100, and 150 μs, and all were used for this analysis. ρ was measured by taking the dB difference of the peaks of the Bragg lines and not measuring the power in adjacent filters. This produces no errors as long as there is no broadening of the Bragg lines, which there did not appear to be for the integration time used. ζ likewise was measured by scaling from the strongest Bragg line peak to the level near zero Doppler which represented an average power level in this region. The nomograph was then used to calculate Δ, the number of dB the omnidirectional sea spectrum is down from the traditional Phillips Ω^{-5} asymptote, which crosses -33 dB $m^2/$Hz at a one-hertz frequency. It is Δ which is then plotted as a function of radar frequency used for comparison with buoy records. The Phillips asymptote for $\alpha = 0.0081$ is drawn on the buoy records of Figs. 8-10, as well as lines 5 and 10 dB down, so that wave power spectral
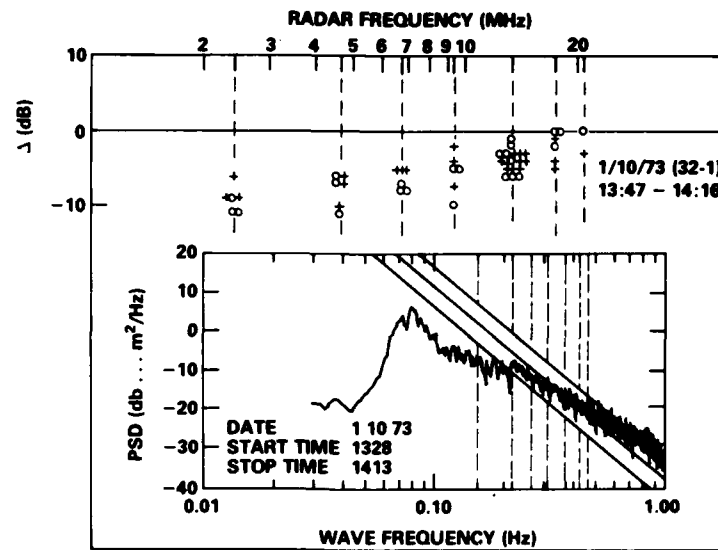
Fig. 8 — Measured values of Δ determined from radar data, using the nomograph of Fig. 4 are plotted versus radar frequency. These are equivalently, 10 log(α_{MEAS}/0.0081), so that each of the points is an estimate of the number of decibels the ocean wave spectrum is down from the traditional Phillips asymptote at the Bragg resonant ocean wave frequency (given roughly by f_B (Hz) = 0.102$\sqrt{f_{radar}}$ (MHz). Circles denote the right of two beams, while crosses denote the left beam. Radar spectra which were noisy at zero Doppler were not used. Below these data is an ocean wave spectrum taken simultaneously within the scattering area using a Waverider buoy. Dotted lines are drawn through the Bragg resonant wave frequencies for each radar frequency running left to right. Wave amplitude differences from the top near-diagonal line representing the Phillips asymptote (α = 0.0081) are to be compared with radar-determined Δ for each frequency from left to right in corresponding order. The lower two diagonal straight lines are down 5 and 10 dB from the Phillips asymptote, respectively.
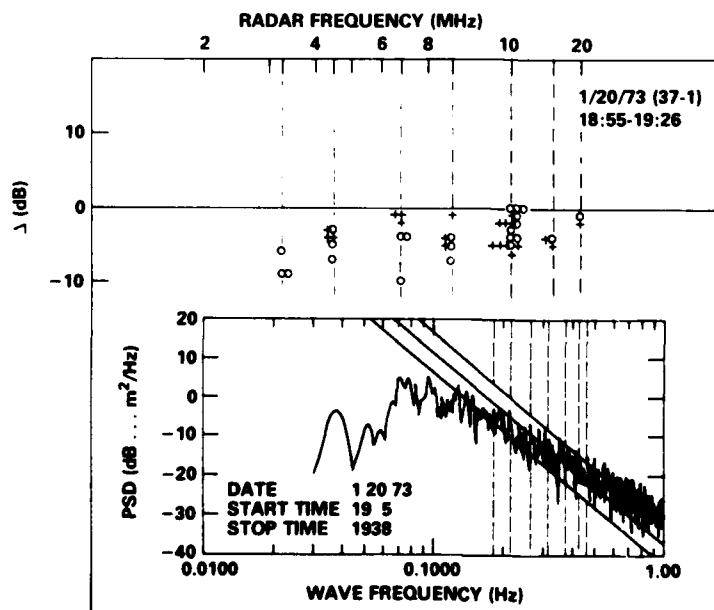
Fig. 9 — Data for a second day for which near simultaneous radar and buoy data are available for comparison, for a case closer to saturation than that in Fig. 8.
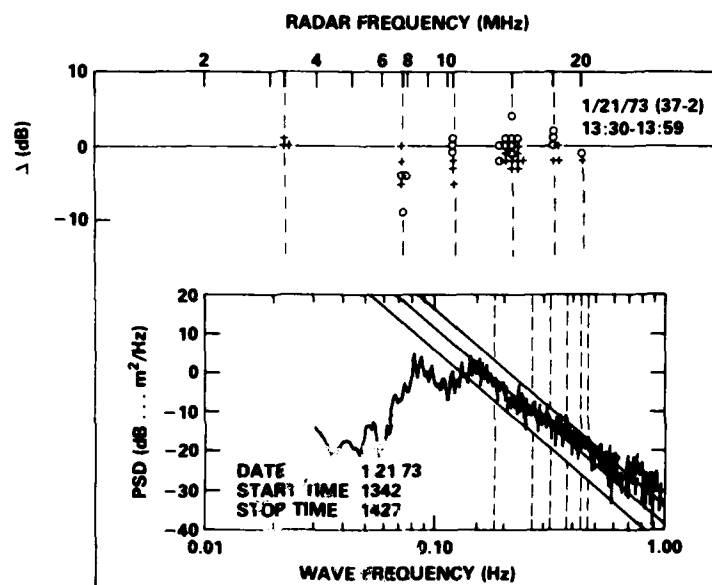
16

Fig. 10 — Data sim... to Figs. 8 and 9, but for a case even closer
to the Phillips saturation reference.

value differences from the Phillips asymptote can be compared directly with the value of Δ derived from the radar data for each Bragg wave frequency.

Figure 8 shows the results of such a comparison for nine frequencies, three of them grouped within 20 kHz of one another near 13.4 MHz. Right and left beam data are plotted separately, and are a good indication of the self-consistency of the analysis. The data for the 24-MHz frequency were omitted because the noise level was higher than the zero Doppler continuum and no value of Δ could be determined. This was also the case for the second and third range bin for the 20-MHz data, due to surface wave propagation losses lowering the signal relative to the noise. Dotted lines are drawn indicating the Bragg ocean wave frequencies sensed by each of the radar frequencies in the buoy spectrum below. The buoy was in the center of one of the radar cells, and the spectrum was taken at the time indicated. The value of Δ determined from each of the two beam positions is indicated by different symbols. The general overlap of the two types of symbols indicates that the spreading function model used in determining the nomograph is not unreasonable, since both beam positions give similar and independent values of Δ. The average value of Δ for each radar frequency is to be compared with the number of dB the corresponding ocean wave power level is down from the Phillips asymptote, based upon a value of α of 0.0081 in the theory. Generally, the agreement is quite good, particularly at the higher frequencies where the spreading function model can be expected to hold rather well. The worst disagreement is for the lowest radar and wave frequency and is probably due to the spreading being much narrower than that assumed in the model. Note the complex behavior of this wave spectrum with ocean wave frequency, a very good example of a case which could not be fit by a model such as the JONSWOP. Note that any inversion techniques for determining wave parameters from radar parameters which depend upon a given model in implementing the technique would have problems with this spectrum.

A second example is shown in Fig. 9, which is much closer to the Phillips asymptote than the previous case. Again data were not available for the 24 MHz frequency and some data points are omitted for other radar frequencies also, because of noise overwhelming the zero Doppler region. Again the agreement is quite good with the worst case being the lowest radar frequency.

17

The third example shown in Fig. 10 is for the case closest to saturation of the three. Again data were omitted when noise precluded a ζ measurement. The agreement between the two data sets is again quite good.

A fourth example is shown in Fig. 11 for a case of cross wind data for one of the look angles, but for which there were no wave records collected. The point of this data is to show that the technique appears to predict consistent results for the highest frequencies, where both sets of data for the two look angles appear distributed similarly. As one drops in radar frequency, the results for the two beams tend to diverge, indicating again that the angular spreading of the directional spectrum is probably narrower for the lower frequencies than is described by theory, and may affect the cross wind case in a more severe manner than other cases for the lower frequencies.
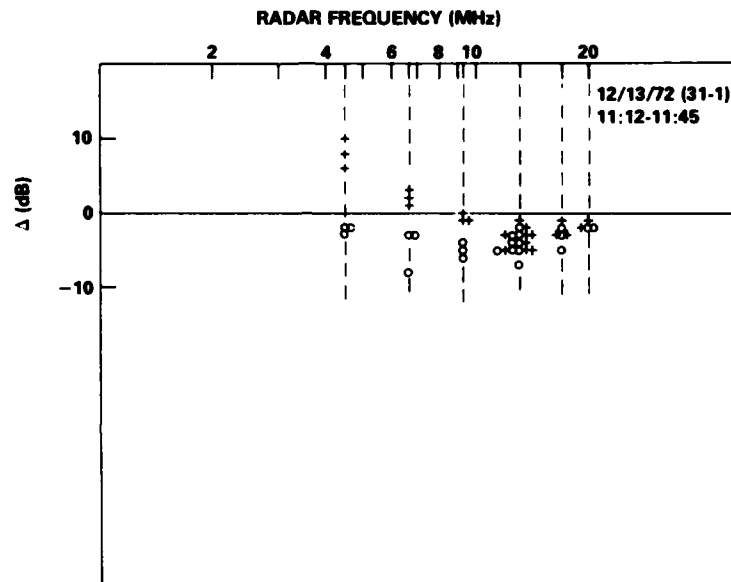
RADAR FREQUENCY (MHz)

Fig. 11 — Data similar to the last three figures, but for which no buoy spectra were available. These data are of interest, however, because of the fact that the crosses represent cases for radar wind angles near ninety degrees. It gives some estimate of where the nomograph accuracy becomes poor, as determined from the poorer self-consistency of the data, as described in the text.

σ^0 ESTIMATION FROM Δ MEASUREMENT

The value of the radar cross section of the sea surface can now be estimated using the inferred value of Δ from the preceeding analysis. It is simply the value of σ^0 from Fig. 6 for the cosine squared plot at zero degrees, -26.9 dB, less Δ, less the angular term due to the spreading function used in the theory, the solid curve of Fig. 7. In the last term we also account for the second Bragg line, which is important for near cross wind conditions. (Strictly speaking, one should also include the second-order continuum, since σ^0 is defined as the sum over all Doppler frequencies of energy scattered from the sea. However, the second-order scatter is far less than either of the two Bragg first-order terms and will be neglected here.) One can then write an equation for σ^0:

$$\sigma^0(\theta) = \sigma^0(0) + \Delta + G(\theta), \tag{19}$$

where the model of Eq. (17) is used for 360 degree spreading:

$$G(\theta) = 10 \log [F(\theta) + F(\theta + \pi)] \tag{20a}$$

$$= 10 \log F(\pi/2) + 10 \log [F(\theta)/F(\pi/2) + F(\theta + \pi)/F(\pi/2)] \tag{20b}$$

$$= - 12 \, dB + \rho/2 * 10 \log [1 + F(\theta + \pi)/F(\theta)] \tag{20c}$$

$$= - 12dB + \rho/2 * 10 \log [1 + 10^{-\rho/10}]. \tag{20d}$$

Note that the second part of the last term will only be important for cases near crosswind when both Bragg lines contribute nearly equally. Otherwise, this term is small and σ^0 will be determined by the amplitude of the strongest Bragg line. Using the value of -26.9 dB for the upwind value of σ^0 gives

$$\sigma^0(\theta) = - 38.9 + \Delta + (\rho/2) * 10 \log [1 + 10^{-\rho/10}]. \tag{21}$$

APPLICATION TO ESTIMATION OF TARGET CROSS SECTION

As a final example of application of the technique, we estimate σ^0 for a case of skywave propagation in which a target is seen, most probably a ship, and estimate its cross section. Figure 12 shows the radar spectrum, collected with a 17-s integration time and a 21.8-MHz radar frequency, at a range of about 1600 km. The two Bragg lines are separated by just a few dB, indicating near cross wind conditions, and ζ is some 16 dB below the strongest Bragg line. From the nomograph, ζ for this case is 24 dB for the 200-s integration time. The correction due to the 17-s integration time is the log of the ratio, 17/200, about 10 dB, yielding a theoretical ζ of 14 dB, which is 2 dB larger than the measured value. Hence a value of Δ of -2 dB is obtained.
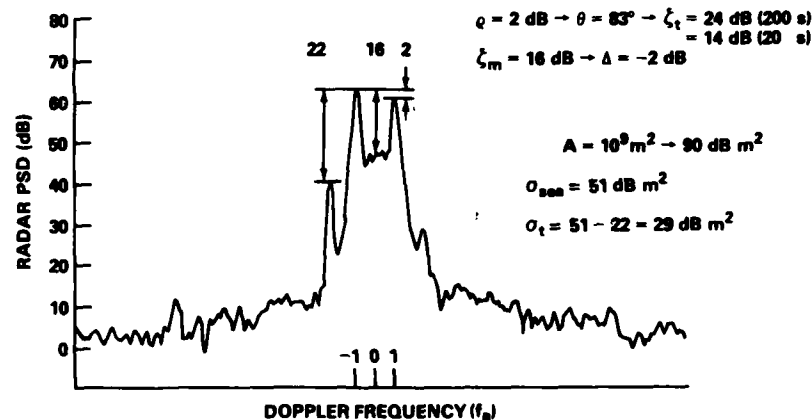

Fig. 12 — An example spectrum is shown in which a ship target return is separated from the clutter, with its cross section estimated from the determination of Δ and σ^0, using the technique developed here. Note that these values for σ^0 and the cross sections do not include the additional 12 dB some authors add for skywave propagation. By our convention, skywave and surface wave cross sections are identical, and the 12 dB is added as a propagation gain to account for the received power increase of 12 dB for skywave cases.

Using the results derived up to this point, we now estimate σ^0 for the example of Fig. 12, where $\Delta = -2$ dB and $\rho = 2$ dB. It follows from Eq. (21) that, for $\Delta = -2$ dB and $\rho = 2$ dB:

$$\sigma^0(\theta) = - 38.9 - 2 + 1*(2.12) = - 38.8 \text{ dB } m^2/m^2. \tag{22}$$

The scattering cell for the pulse length and beam width used was of the order of 90 dB above a square meter, so that the sea surface scattering cross section was 51.2 dB m^2. The value of the cross section of the target is then scaled from this amplitude of the greater Bragg peak, which is 22 dB higher, and is

19

therefore 29.2 dB above a square meter, or 832 m^2. *Note that some authors add 12 dB to the cross section for skywave propagation to account for the antenna image and the target image. We choose to include these as propagation effects in the radar equation.*

One is cautioned in applying this technique to target cross section estimation, to be very careful to choose the largest value for the target signal out of a series of Doppler spectra, because polarization fading on targets is far more severe for a small target than the Doppler spectrum of the sea surface. Ideally one should average the Doppler sea echo spectrum for a minimum of 10 min, and take the largest target cross section observed in that time period for comparison.

SUMMARY

We have developed a technique that allows one to estimate the cross section of the sea surface at HF by a very simple measurement of two characteristics of the radar Doppler spectrum: the approach-recede Bragg line ratio, ρ, and the spectral energy ratio of the strongest Bragg line to the average continuum value near zero Doppler frequency, ζ. Using a nomograph, based upon a theoretical model for the Doppler spectrum, one can estimate the scattering cross section per unit area, σ^0, for the observed patch of sea surface being illuminated. The technique therefore does not require any system calibration or knowledge of antenna gain patterns, ionospheric D-region losses, and the like, and so is self calibrating. The technique was applied to radar data collected in the surface wave mode and the results were compared to independent measurements of the omnidirectional sea spectrum made by a Waverider buoy. Since the data agree quite well with one another for the several look angles and ranges that were used for the measurements, the implication is that the model for the spreading function used to develop the nomograph is generally a valid one for most radar frequencies. The data showed a tendency to disagree with the buoy spectra for the lowest radar frequencies, near 2 and 4 MHz, and this is thought to be due to the prevailing directional spreading function not being well represented by the model that was used for these ocean wave frequencies. *The wave spectrum is known to be very narrow for frequencies near the ocean wave spectrum peak, as well as for sea conditions which are newly developing, and our technique should be applied with caution for these cases.* To date, the uncertainty in knowledge of the variability of the spreading function with frequency and changing sea conditions appears to be the biggest uncertainty in understanding the Doppler spectrum at HF. This work is meant to be an introduction to using the radar Doppler spectrum as a cross section calibration, and it is felt to be sufficiently accurate to be applied to most conditions appropriate to ionospheric propagation, in particular the high frequency portion of the HF band. Work will continue in updating and refining techniques introduced here.

ACKNOWLEDGMENT

REFERENCES

1. H.C. Lin and A.A. Ksiensky, "Optimum Frequencies for Aircraft Classification," *Ohio State University Electroscience Laboratory Technical Report 78 3815-6*, 1979.

2. J.L. Ahearn, S.R. Curley, J.M. Headrick, and D.B. Trizna, "Tests of Remote Skywave Measurement of Ocean Surface Conditions," *Proceedings IEEE*, **62**, pp. 681-687, 1974.

3. D.E. Barrick, "First Order Theory and Analysis of MF/HF/VHF Scatter from the Sea," *IEEE Trans. AP*, **AP-20**, pp. 2-9, 1972.

4. C.C. Teague, G.L. Tyler, and R.H. Stewart, "The Radar Cross Section of the Sea at 1.95 MHz: Comparison of In-Situ and Radar Determinations," Radio Science, **10**, pp. 847-852, 1975.

5. N.J. Pierson and L.I. Moskowitz, J. Geophys. Res., **69**, 5181 (1964).

6. K. Hassleman, T.P. Barnett, E. Bouws, H. Carlson, D.E. Cartwright, K. Enke, J.A. Ewing, H. Gienapp, D.E. Hassleman, P. Kruseman, A. Meerburg, P. Muller, D.J. Olbers, K. Richter, W. Sell, and H. Walden, "Measurements of Growth and Swell Decay during the Joint North Sea Wave Project (JONSWAP)," Deutsches Hydrographisches Institut, 1973.

7. A.E. Long and D.B. Trizna, "Mapping of North Atlantic Winds by HF Radar Sea Backscatter Interpretation," IEEE Trans. A.P., **AP-21**, pp. 680-685 (1973).

8. J.W. Mareska and C.T. Carlson, "High-Frequency Skywave Radar Measurements of Hurricane Anita," Science, **209**, 1189-1196, 1980.

9. D.B. Trizna, J.C. Moore, J.M. Headrick, and R.W. Bogle, "Directional Sea Spectrum Determination Using HF Doppler Radar Techniques," IEEE Trans., AP, **AP-25**, pp. 4-11, 1977.

10. D.E. Barrick, "Remote Sensing of Sea State by Radar," in *Remote Sensing of the Troposphere*, V.E. Derr, ed., U.S. Gov. Printing Office, August 1972.

11. G.R. Valenzuela, "The Effect of Capillarity and Resonant Interactions on the Second-Order Doppler Spectrum of Radar Sea Echo," J. Geophys. Res., **79**, pp. 5031-5037, 1974.

12. R.B. Leighton, *Principles of Modern Physics*, McGraw-Hill, 795, 1959.

13. W. Heitler, "The Quantum Theory of Radiation," Oxford Press, London, 1954.

14. D.B. Trizna, R.W. Bogle, J.C. Moore, and C.M. Howe, "Observation by HF Radar of the Phillips Resonance Mechanism for Generation of Wind Waves," J. Geophys. Res., **85**, pp. 4946-4956, 1980.